Rod Formation of Ionic Surfactants: Electrostatic and Conformational Energies

Armin Bauer

Department of Applied Mathematics, Research School of Physical Sciences and Engineering, Australian National University, Canberra 0200, ACT, Australia

Stefan Woelki and Hans-Helmut Kohler*

University of Regensburg, Institute of Analytical Chemistry, Chemo- and Biosensors, D-93040 Regensburg, Germany

Received: July 17, 2003; In Final Form: November 10, 2003

We present a thermodynamic model that describes the formation of micelles from ionic surfactants in aqueous solution at varying counterion concentrations. The micellar aggregates may be spheres, dumbbells, and rods. A former theory [Heindl, A.; Kohler, H.-H. *Langmuir* **1996**, *12*, 2464] is refined by the introduction of detailed models for the conformational energy of the surfactant chains and the electrostatic interaction of the ionic headgroups. The standard Gibbs energy of a surfactant ion is minimized under constraints imposed by the micelle shape. The conformational energy is calculated from an appropriately modified single-chain mean-field model proposed in another work [Ben-Shaul, A.; Gelbart, W. M. In *Membranes, Microemulsions and Monolayers*; 1994]. For the electrostatic interactions, we use a previously developed local balance model for a charged interface [Woelki, S.; Kohler, H.-H. *Chem. Phys.* **2000**, *261*, 411-419; 421−438]. This leads to a marked counterion specificity of the standard Gibbs energies of the micelles. Interfacial tension, steric headgroup repulsion, and direct counterion adsorption are taken into consideration. From the standard Gibbs energies, the size distribution of the micelles can be obtained by application of the law of mass action. This distribution is used to calculate the viscosity of the micellar solution at a given concentration of surfactant and salt. A single fitting parameter—the counterion dissociation constant—is used to fit the model to experimental viscosity data for cetylpyridinium chloride, bromide, iodide, and nitrate. It is shown that two alternative models for the shape of the rods can be used to explain the observed counterion specificity.

1. Introduction

Micellization in an aqueous solution of the cationic surfactant cetylpyridinium (Cp^+)—as of any ionic surfactant—is strongly influenced by the nature and concentration of the counterion. This can be seen, for instance, in viscosity measurements.[1] In general, solutions of the pure surfactant obey Einstein's viscosity law, indicating that the micelles are spheres. When the counterion concentration is increased by adding sufficient amounts of salt, the viscosity of the solution strongly increases, because of a transition from spherical to rodlike micelles of increasing length. Micelle growth is very sensitive to the counterion species and to counterion concentration. In the case of the chloride and iodide, for instance, counterion concentrations of as much as 2.5 mol L^{-1} and as little as 6×10^{-3}mol L^{-1}, respectively, produce similar viscosity effects. Further results of viscosity measurements are found in the work by Ekwall et al.,[2] Porte et al.,[3] Gamboa and co-workers,[4,5] and Zoeller and Blankschtein.[6] Counterion specific phenomena are also observed for other aggregation properties, such as the critical micelle concentration.[7,8]

Other experimental methods, such as light scattering, small-angle X-ray scattering, and small-angle neutron scattering, can be used to investigate the distribution of micelles and micellar parameters.[6−16] The sphere-to-rod transition can be made visible by cryogenic transmission electroscopy, where even the endcaps of the rods can be seen.[17−19]

Theoretical approaches that describe micellization are usually based on the general thermodynamic principles of self-aggregation. In more sophisticated cases, the interactions—mainly of hydrophobic, steric, conformational and electrostatic origin—are treated on a molecular level.[20−29]

This paper starts from a previous theory[30] of the formation of spherical and rodlike micelles; this theory combines a micelle formation model with a viscosity model. In the previous theory, the micelle formation model is used to calculate the size distribution of the micelles at a given composition of the solution, which then is used to calculate the viscosity of the solution from the viscosity model. In this way, the viscosity of dilute surfactant solutions is calculated as a function of surfactant and counterion concentration. The results of the theory are compared with experimental viscosity results for Cp^+ solutions with chloride, bromide, iodide, and nitrate as counterions. In the micelle formation model of the previous theory, spheres, dumbbells, and rods are used as micellar geometries. It is an essential feature of that model that, for a given aggregation number, the inherent geometrical parameters (the radii of spherical and cylindrical parts) are obtained by minimizing the Gibbs energy of the micelle. The conformational energy of the surfactant chains is taken into consideration indirectly, by

* Author to whom correspondence should be addressed. E-mail: Hans-Helmut.Kohler@chemie.uni-regensburg.de.

10.1021/jp036088v CCC: $27.50
Published on Web 01/16/2004

introducing a hypothetical curvature dependence of the interfacial tension hydrocarbon/water, whereas the electrostatic energy of the charged interface is calculated from the Poisson−Boltzmann−Stern equation with low curvature approximations for spherical and cylindrical geometries.[31] In the previous theory, counterion specificity is mainly based on different dissociation constants of direct counterion adsorption. There are other adjustable parameters; among them are three curvature parameters in the expression for the interfacial tension between hydrocarbon and water, and two Stern layer parameters are used in the Poisson−Boltzmann−Stern ansatz. These adjustable parameters are used to fit the model to the experimental viscosity data.

A weak point of the previous theory exists, in that the free parameters and their fitted values lack immediate physical significance. Therefore, the results of that theory are rather speculative. It is the intent of the present paper to reformulate the model and eliminate all these free parameters, with the only exception of the dissociation constant of counterion adsorption. A realistic molecular model for the conformational energy of a surfactant chain and a more-detailed model for the electrostatic energy of the charged interface will be used. This way, the physical basis of the overall theory of micelle formation will be greatly improved.

Furthermore, this paper represents an approach to understand the physics behind counterion-specific, or "Hofmeister", effects. It is known that classical Poisson−Boltzmann models cannot account for a comprehensive description of counterion specific systems.[32] This raises the question of which effects actually determine counterion specificity. The electrostatic theory used in this paper takes various effects into consideration, such as dielectric saturation, excluded volume, and self-atmosphere potentials. These effects have been shown to lead to marked counterion-specific values for the electrostatic energy of the charged interface.[33,34] By incorporating the new electrostatic theory into the micelle formation model, the significance of these effects, in terms of counterion specificity, will be assessed.

2. Model

2.1. Thermodynamics of Micellization. We consider an equilibrium state of an ideal surfactant solution that contains micelles of different shape and size. The micelles may be spheres, dumbbells, and rods. The pressure and the absolute temperature (T) are assumed to be constant. A micelle of aggregation number n (M_n) is regarded as a chemical species formed from n surfactant molecules A:

$$n\mathrm{A} \rightleftarrows \mathrm{M}_n \qquad (n = 2, 3, ...) \tag{1}$$

The law of mass action of this reaction may be written as

$$\frac{c_M(n)}{c_0} = \left(\frac{c_A}{c_0}\right)^n K_M(n) = \left(\frac{c_A}{c_0}\right)^n \exp\left(-\frac{G_M(n)}{kT}\right) \tag{2}$$

where c_A is the molar concentration of the monomer, $c_M(n)$ the molar concentration of micelles of aggregation numer n, and $K_M(n)$ the equilibrium constant. The standard concentration (c_0) is chosen to be the surfactant concentration in the condensed state; that is,

$$c_0 = \frac{1}{N_{Av} v_A} \tag{3}$$

where N_{Av} is Avogadro's constant and v_A is the volume of a surfactant chain.

Micelles may consist of parts of a different geometry $\mathcal{G}$. A rod-shaped micelle, for instance, may be considered to consist of a cylindrical part and two spherical endcaps. We use $g_{\mathcal{G}}$ to denote the Gibbs standard energy for the transfer of a surfactant molecule from the solution into a region of geometry $\mathcal{G}$. The Gibbs energy of an aggregate M_n ($G_M(n)$) is assumed to be the sum of the Gibbs standard energies of the surfactant molecules in the different micellar parts. Thus,

$$G_M(n) = \sum_{\mathcal{G}} n_{\mathcal{G}} g_{\mathcal{G}} = n\bar{g} \tag{4}$$

where $n_{\mathcal{G}}$ is the number of surfactant molecules in a part of geometry $\mathcal{G}$ and $\bar{g}$ is the mean standard Gibbs energy of a surfactant molecule within the micelle as a whole. For a given type of micelle and a given n, $G_M(n)$ is minimized to determine the optimal type of geometry and the corresponding geometrical parameters. Details of the minimization concept and the different micelle types are given later.

$G_M(n)$ can be written as

$$G_M(n) = n g_c^{\infty} + \Delta G_{rod}(n) \tag{5}$$

where g_c^{∞} is the standard Gibbs energy of a surfactant molecule within what we call the reference cylinder. This is an infinitely long cylinder whose energy is minimized, with respect to g_c. $\Delta G_{rod}(n)$ is the energy required to form a micelle M_n from n surfactant molecules that have been removed from this reference cylinder. For a rod-shaped micelle, for instance, $\Delta G_{rod}(n)$ is the energy required to transform n surfactant ions taken from the reference cylinder into a rod-shaped micelle with endcaps. In general, the diameter of the cylindrical portion of the rod will be different from that of the reference cylinder; therefore, $\Delta G_{rod}(n)$ includes the energy for the radial reshaping of the cylindrical portion.

From eqs 4 and 5, we obtain

$$\Delta G_{rod}(n) = (\bar{g} - g_c^{\infty})n \tag{6}$$

With eq 5, eq 2 now becomes

$$\frac{c_M(n)}{c_0} = \left(\frac{c_A}{c_0}\right)^n \exp\left(-\frac{g_c^{\infty}}{kT}\right)^n \exp\left(-\frac{\Delta G_{rod}(n)}{kT}\right) \tag{7}$$

Defining the characteristic (or critical) micelle concentration for the formation of a cylindrical micelle by

$$\mathrm{cmc}_c = c_0 \exp\left(\frac{g_c^{\infty}}{kT}\right) \tag{8}$$

we obtain

$$\frac{c_M(n)}{c_0} = \left(\frac{c_A}{\mathrm{cmc}_c}\right)^n \exp\left(-\frac{\Delta G_{rod}(n)}{kT}\right) \tag{9}$$

where cmc_c will be identified with the experimental value of the critical micelle concentration. Equation 9 shows that, at a given ratio c_A/cmc_c, the distribution over n is determined by the value of $\Delta G_{rod}(n)$.

For a given aggregation number n, different types of micelles (spheres, dumbbells, rods) can be constructed with different values of $\Delta G_{rod}(n)$. If only the aggregate with the lowest value is taken into consideration, the total molar concentration of surfactant molecules contained in micellar aggregates ($\hat{c}_A$) can be written as

$$\hat{c}_A = \sum_{n=2}^{\infty} n c_M(n) = \sum_{n=2}^{n_{sph}^{max}} n c_{sph}(n) + \sum_{n=n_{sph}^{max}+1}^{n_{dum}^{max}} n c_{dum}(n) + \sum_{n=n_{dum}^{max}+1}^{\infty} n c_{rod}(n) \quad (10)$$

where the abbreviations "sph", "dum", and "rod" denote sphere-, dumbbell-, and rod-shaped micelles, respectively. Note that, in this relation, the smallest micellar aggregate has an aggregation number of $n = 2$. The maximum aggregation numbers for spheres and dumbbells are given by n_{sph}^{max} and n_{dum}^{max}, respectively, where $n_{sph}^{max} \le n_{dum}^{max}$.

The probability of observing a micelle of aggregation number n is

$$p(n) = \frac{c_M(n)}{\sum_{n=2}^{\infty} c_M(n)} \quad (11)$$

whereas the probability of surfactant ions to be observed in a micelle of aggregation number n is

$$p_v(n) = \frac{n c_M(n)}{\sum_{n=2}^{\infty} n c_M(n)} = \frac{n c_M(n)}{\hat{c}_A} \quad (12)$$

2.2. Gibbs Energy of a Surfactant Molecule within a Micelle. According to eq 4, $G_M(n)$ is obtained from the energies $g_{\mathscr{G}}$ of the different parts of the micelle, where each $g_{\mathscr{G}}$ value is calculated, step by step, from the following relation (see ref 30):

$$g_{\mathscr{G}} = g^* + \Delta g_{conf} + \Delta g_{inter} + \Delta g_{ster} + \Delta g_{el|ad} \quad (13)$$

Here, g^* is the energy of a common reference state, which is assumed to have a plane hydrocarbon/water interface with headgroup area a^*.[30] The value of g^* drops out of the equation when $\Delta G_{rod}(n)$ is calculated according to eq 6, so its value does not need to be specified. The parameter Δg_{conf} is the conformational energy of the surfactant chain, whereas Δg_{inter} is the interfacial energy of the hydrocarbon/water interface, Δg_{ster} is the steric headgroup repulsion energy, and $\Delta g_{el|ad}$ is the electrostatic energy of the charged interface (including counterion adsorption). These terms will be explained in detail below.

2.2.1. Conformational Energy of the Surfactant Chain. For the calculation of Δg_{conf}, we follow the mean field approach that was proposed by Ben-Shaul and Gelbart.[35] In this approach, the free energy of a surfactant chain packed into a micelle core is minimized under specific requirements, accounting for shape (cylinder, sphere), size (micelle radius), and composition (uniform liquid hydrocarbon) of the micelle core. The packing conditions reduce the translational and the conformational degrees of freedom of the chain and create a marked dependence of Δg_{conf} on geometry.

TABLE 1: Fit Parameters, According to eq 14, for a Cylinder and a Sphere, as a Function of Chain Length

chain length	c_0	c_1	c_2	c_3	c_4
		Cylinder			
10	0.5299	27.483	35.443	−22.214	5.6467
12	−0.2099	−24.431	27.106	−14.668	3.2434
14	−0.2065	−24.696	24.585	−11.752	2.2694
16	−1.4541	−21.784	19.719	−8.622	1.5254
		Sphere			
10	6.1977	−34.570	34.050	−16.232	3.1548
12	6.8531	−36.701	34.770	−15.921	2.8692
14	9.8350	−44.791	40.815	−17.360	2.8510
16	5.4955	−31.342	24.342	−8.986	1.3054

In ref 35, the micelle core is modeled in the form of concentric layers. One end of the surfactant chain is randomly placed at different positions within a small interval, perpendicular to the micelle surface. For its overall orientation, 12 first-bond vectors that lead from the headgroup to the first methylene segment are randomly sampled. Finally, the internal bond sequences are generated according to the rotational isomeric state (ris) approximation, which leads to a large number of chain conformations. For a conformation to be admitted, each chain segment must lie in one of the layers of the micelle core. The segment is attributed to the layer that accommodates its center of mass. To prevent self-overlap of chain segments within a chain, conformations with consecutive gauche$^+$/gauche$^+$ or gauche$^-$/gauche$^-$ internal bond sequences are discarded.

Our calculations have shown that the model needs refinement to provide smooth curves for Δg_{conf} as a function of the micellar radius R or the headgroup area a. Thus, the first step was to increase the number of first-bond vectors. A more important improvement was obtained by representing a chain segment as a sphere and attributing each volume element of the sphere to its respective layer. Thus, a single segment can contribute to more than one layer. A more-detailed description of our procedure to determine chain conformations is found in the Appendix.

From the model calculations, we generated least-squares fits for Δg_{conf}, as a function of the radius R, using the following expansion:

$$\frac{\Delta g_{conf}}{kT} = c_0 + c_1\left(\frac{R}{\text{nm}}\right) + c_2\left(\frac{R}{\text{nm}}\right)^2 + c_3\left(\frac{R}{\text{nm}}\right)^3 + c_4\left(\frac{R}{\text{nm}}\right)^4 \quad (14)$$

where $c_0 \cdots c_4$ are the fit parameters. Their values are listed in Table 1, as a function of chain length for cylindrical and spherical geometries.

2.2.2. Interfacial Energy of the Hydrocarbon/Water Interface. The interfacial energy of the hydrocarbon/water interface (Δg_{inter}) is obtained from the relation

$$\Delta g_{inter} = \sigma(a - a_*) \quad (15)$$

where a is the area per surfactant molecule and a_* is the area in the reference state. The interfacial tension between the hydrocarbon and the water (σ) is given as a function of temperature T and molar mass M of the hydrocarbon chain by[25]

$$\sigma = \sigma_A + \sigma_W - 1.1\sqrt{\sigma_A \sigma_W}$$

$$\sigma_W = \left[72.0 - 0.16\left(\frac{T}{\text{K}} - 298\right)\right] \text{mN/m}$$

$$\sigma_A = \left[35.0 - 325\left(\frac{M}{\text{g mol}^{-1}}\right)^{-2/3} - 0.098\left(\frac{T}{\text{K}} - 298\right)\right] \text{mN/m} \quad (16)$$

where σ_W is the interfacial tension between water and air and σ_A is the interfacial tension between the hydrocarbon and air. At $T = 323.15$ K, the interfacial tension of hexadecane is $\sigma = 47.5$ mN/m.

2.2.3. Steric Headgroup Repulsion Energy. The steric headgroup pressure is described by the VOLMER equation:[36]

$$\pi = \frac{kT}{a - a_0} \tag{17}$$

where a_0 is the excluded headgroup area. For pyridinium, a value of $a_0 = 0.375$ nm^2 is used.[30] Integration of the last equation gives the steric headgroup repulsion energy, Δg_{ster}:

$$\Delta g_{ster} = -\int_{a_*}^{a} \pi \, da = -kT \int_{a_*}^{a} \frac{1}{a - a_0} \, da$$
$$= -kT \ln\left(\frac{a - a_0}{a_* - a_0}\right) \tag{18}$$

2.2.4. Electrostatic Energy of the Charged Interface including Counterion Adsorption. In the former micelle formation model, the electrostatic energy of the surfactant ion was calculated from the ordinary Poisson−Boltzmann−Stern theory, neglecting volume effects, dielectric saturation, etc. As mentioned, solutions for cylindrical and spherical geometries were based on low curvature approximations;[31] however, the actual curvature was rather high. In the present model, we use a local balance model of the electrical double layer recently proposed by Woelki and Kohler.[33,34] This model provides numerical solutions of the system of differential equations that result from the Poisson equation and the thermodynamic equilibrium conditions (constant electrochemical potentials). In the Woelki model, the following effects which are not—or are only approximately—covered by the ordinary Poisson−Boltzmann−Stern theory are taken into consideration: (i) excluded volumes of the solutes, (ii) dependence of the permittivity of the solution on composition and field strength (dielectric saturation), (iii) self-atmosphere potentials and image forces, and (iv) curvature effects.

In Figure 1, the electrostatic energies per cetylpyridinium (Cp^+) ion obtained from the previous model (Δg_{pb}) and the new model (Δg_{el}) are plotted as a function of the micelle radius R for various counterions. Results are shown for cylindrical and spherical geometries. Evidently, the counterion specificity is strongly enhanced in the new model. which is due to a synergism that involves dielectric saturation and effective partial molar volumes.[34,37] In principle, the model includes self-atmosphere potentials and image forces, according to the Bell−Levine theory.[38] However, these effects were determined to be of little importance and, therefore, are neglected in this paper.

For the purpose of the micelle formation model, we additionally incorporate direct counterion adsorption to the micelle surface. Adsorption is assumed to follow the Langmuir adsorption isotherm:

$$\theta = \frac{c_B(H)}{c_B(H) + K_{diss}} \tag{19}$$

where θ is the degree of counterion adsorption, $c_B(H)$ the concentration of counterions in front of the Helmholtz layer, and K_{diss} the dissociation constant. K_{diss} is used to fit the rod-formation model to the viscosity data. Note that the Langmuir ansatz mainly serves as a simple tool to account for further ion specific effects that are not covered by the current electrostatic model.

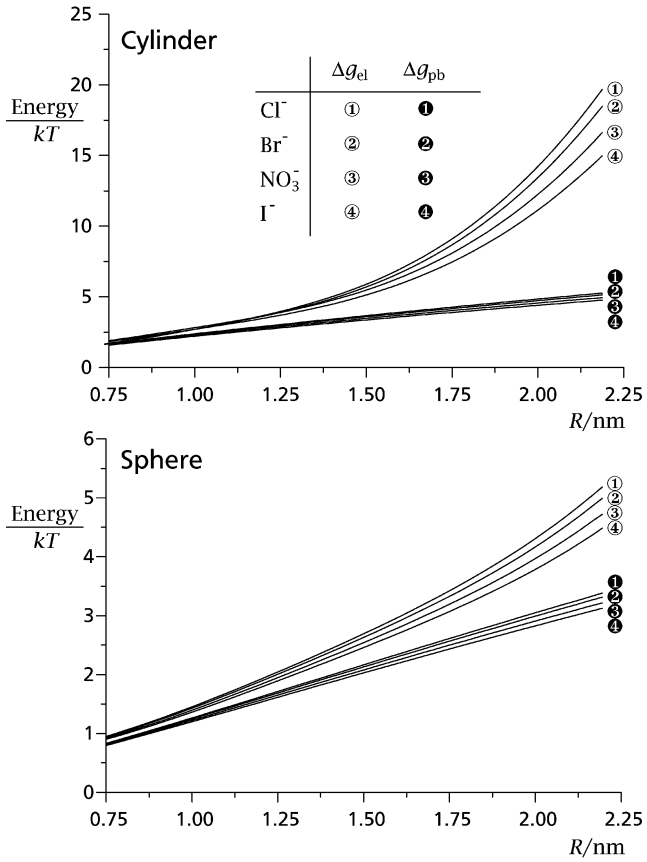

Figure 1. Electrostatic energy per surfactant ion of the new model (Δg_{el}) and that of the ordinary Poisson−Boltzmann−Stern theory (Δg_{pb}) for cetylpyridinium (Cp^+) micelles with various counterions. Energies are plotted as a function of radius R for cylindrical and spherical geometries. The counterion concentration is 0.5 mol L^{-1} in all curves.

With adsorption, the electrostatic energy of the surfactant ion ($\Delta g_{el|ad}$) is[30]

$$\Delta g_{el|ad} = \Delta g_{el} + kT \ln(1 - \theta) + e_o \varphi_o \theta \tag{20}$$

where φ_o is the surface potential, e_o the elementary charge, and Δg_{el} the electrostatic energy of a surfactant ion of effective ionic charge $e_o(1 - \theta)$.

With the inclusion of the new electrostatic model, the counterion effects calculated from the micelle formation model become much more distinct than they were before. Apart from that, cylindrical and spherical geometries now are calculated without resorting to low-curvature approximations.

3. Micellar Geometry and Minimization Concept

Figure 2 provides an overview of the micellar geometries used in this paper. All energy minimizations described in the following are performed numerically.

3.1. Cylindrical Micelle. In our approach, a cylindrical micelle is a section of a rod-shaped micelle. The volume (V_c) and area (A_c) of a cylindrical micelle of aggregation number n_c are given by the following equations:

$$V_c = n_c v_{chain} = \pi r_c^2 l_c \tag{21a}$$

$$A_c = n_c a_c = 2\pi r_c l_c \tag{21b}$$

where r_c, l_c, and a_c are the respective radius, length, and headgroup area of the cylindrical micelle, and v_{chain} is the

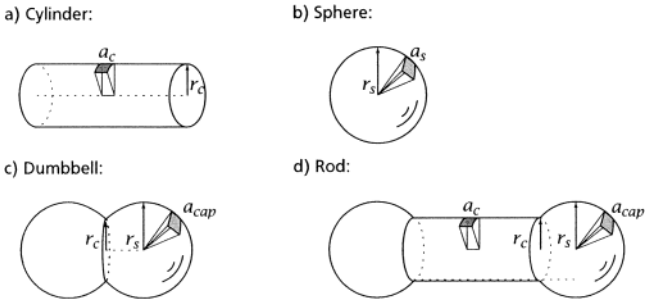

Figure 2. Schematic representation of micellar species.

volume of the surfactant chain. Dividing eq 21a by eq 21b leads to a relation that no longer contains n_c:

$$r_c = \frac{2v_{chain}}{a_c} \tag{22}$$

The parameter v_{chain} is constant; therefore, a_c is a function of r_c alone and vice versa. The radius of the infinitely long cylindrical micelle with minimum energy is obtained from the relation

$$\frac{dg_c^\infty}{dr_c} = 0 \tag{23}$$

The minimum value of g_c^∞ is needed for the calculation of ΔG_{rod} in eq 12.

3.2. Spherical Micelle. The volume (V_s) and area (A_s) of the spherical micelle of aggregation number n_s are given by the following equations:

$$V_s = n_s v_{chain} = \frac{4}{3}\pi r_s^3 \tag{24a}$$

$$A_s = n_s a_s = 4\pi r_s^2 \tag{24b}$$

Division of eq 24a by eq 24b gives the relation

$$r_s = \frac{3v_{chain}}{a_s} \tag{25}$$

where, according to eqs 24a and 24b, r_s and a_s are functions of n_s. Therefore,

$$G_s(n_s) = n_s g_s(n_s) \tag{26}$$

Thus, at a given n_s, there is no room for any minimization of g_s.

3.3. Dumbbell-Shaped Micelle. The geometry of a dumbbell-shaped micelle is defined by the two radii r_c and r_s (see Figure 2c). The height h of the spherical segment that has to be cut from each of the spheres to form a dumbbell is given by the relation

$$h = r_s - \sqrt{r_s^2 - r_c^2} \tag{27}$$

The volume (V_{dum}) and area (A_{dum}) of the dumbbell-shaped micelle can be expressed as

$$V_{dum} = n_{dum} v_{chain} = 2\left[\frac{4}{3}\pi r_s^3 - \frac{1}{3}\pi h^2(3r_s - h)\right] \tag{28a}$$

$$A_{dum} = n_{dum} a_{dum} = 2(4\pi r_s^2 - 2\pi h r_s) \tag{28b}$$

At given values of n_{dum} and r_c, the radius r_s of the spherical component is given by eq 28a with eq 27. Therefore, G_{dum} can be treated as a function of the independent variables n_{dum} and r_c:

$$G_{dum}(n_{dum}, r_c) = n_{dum} g_{dum}(n_{dum}, r_c) \tag{29}$$

At a given value of n_{dum}, the optimal value of r_c is determined from the minimization condition:

$$\frac{\partial g_{dum}}{\partial r_c}\Big|_{n_{dum}} = 0 \tag{30}$$

3.4. Rod-Shaped Micelles. Two types of rod-shaped micelles of identical shape are used: type 1 and type 2. In type 2, the headgroups are allowed to move between the cylindrical and spherical components, whereas in type 1, they are not.

3.4.1. Type 1. The rod-shaped micelle of type 1 is composed of a cylindrical component and two hemispherical endcaps (see Figure 2d). The volume (V_{rod}) and surface (A_{rod}) are calculated from the following equations:

$$V_{rod} = n_{rod} v_{chain} = (n_c + n_{cap}) v_{chain} = V_c + V_{cap} \tag{31a}$$

$$A_{rod} = n_c a_c + n_{cap} a_{cap} = A_c + A_{cap} \tag{31b}$$

If n_{rod}, r_c, and r_s are given, all quantities that appear in these equations can be calculated from previous equations (in eqs 28a and 28b, the index "dum" must be replaced by "cap"). Therefore, n_{rod}, r_c, and r_s are independent variables:

$$\begin{aligned} G_{rod}(n_{rod}, r_c, r_s) &= n_c g_c(n_{rod}, r_c, r_s) + n_{cap} g_{cap}(n_{rod}, r_c, r_s) \\ &= n_{rod}\, \bar{g}_{rod}(n_{rod}, r_c, r_s) \end{aligned} \tag{32}$$

With n_{rod} given, the radii r_c and r_s of the rod-shaped micelle of minimum energy are obtained from the following conditions:

$$\frac{\partial \bar{g}_{rod}}{\partial r_c}\Big|_{n_{rod}, r_s} = 0 \tag{33a}$$

$$\frac{\partial \bar{g}_{rod}}{\partial r_s}\Big|_{n_{rod}, r_c} = 0 \tag{33b}$$

3.4.2. Type 2. In this type, the headgroup of the surfactant ion is assumed to be cut off from the hydrocarbon tail. Therefore, the headgroup aggregation numbers of the cylindrical and hemispherical parts, n_c^{hd} and n_{cap}^{hd}, may differ from n_c and n_{cap}. The headgroup areas are

$$a_c^{hd} = \frac{A_c}{n_c^{hd}}$$

$$a_{cap}^{hd} = \frac{A_{cap}}{n_{cap}^{hd}} \tag{34}$$

Because of the mobility of the headgroups, n_{cap}^{hd} is an additional

independent variable. We split g into a chain term (g^{ch}) and a headgroup term (g^{hd}):

$$g^{ch} = \Delta g_{conf}(r) \tag{35a}$$

$$g^{hd} = \Delta g_{inter}(a^{hd}) + \Delta g_{ster}(a^{hd}) + \Delta g_{el|ad}(r,a^{hd}) \tag{35b}$$

Thus,

$$G_{rod}(n_{rod},r_c,r_s,n_{cap}^{hd}) = n_c^{hd}g_c^{hd} + n_c g_c^{ch} + n_{cap}^{hd}g_{cap}^{hd} + n_{cap}g_{cap}^{ch} = n_{rod}\bar{g}_{rod}(n_{rod},r_c,r_s,n_{cap}^{hd}) \tag{36}$$

where $n_c^{hd} = n_{rod} - n_{cap}^{hd}$.

For a given value of n_{rod}, the optimal values of r_c, r_s, and n_{cap}^{hd} are determined from

$$\frac{\partial \bar{g}_{rod}}{\partial r_c}\Big|_{n_{rod},r_s,n_{cap}^{hd}} = 0 \tag{37a}$$

$$\frac{\partial \bar{g}_{rod}}{\partial r_s}\Big|_{n_{rod},r_c,n_{cap}^{hd}} = 0 \tag{37b}$$

$$\frac{\partial \bar{g}_{rod}}{\partial n_{cap}^{hd}}\Big|_{n_{rod},r_c,r_s} = 0 \tag{37c}$$

4. Viscosity Model

The relative viscosity of the solution (η_{rel}) is given by

$$\eta_{rel} = \frac{\eta}{\eta_{cmc}} = 1 + \Delta\eta_{rel}^{sph} + \Delta\eta_{rel}^{rod} \tag{38}$$

where η and η_{cmc} are the viscosities of the actual solution and the solution at the critical micelle concentration (cmc). The viscosity contributions of spheres and rods ($\Delta\eta_{rel}^{sph}$ and $\Delta\eta_{rel}^{rod}$, respectively) are determined theoretically from the micelle distribution obtained from the micelle formation model (see eq 18).

For $\Delta\eta_{rel}^{sph}$, we employ Einstein's viscosity law for spherical particles:

$$\Delta\eta_{rel}^{sph} = 2.5\Phi_{sph} \tag{39}$$

where Φ_{sph} is the volume fraction of the spherical micelles. Note that Φ is related to p_v by the relation $\Phi(n) = (\hat{c}_A/c_0)p_v(n)$.

The parameter $\Delta\eta_{rel}^{rod}$ is determined from

$$\Delta\eta_{rel}^{rod} = 0.25\Phi_{rod}\left\{\frac{\langle f^2\rangle_v}{\ln[0.63(\langle f^3\rangle_v/\langle f^2\rangle_v)]}\right\} \tag{40}$$

where Φ_{rod} is the total volume fraction of the rods. The angular brackets indexed with the symbol "v" denote a volume average calculated from the probability distribution of eq 18. Equation 40 applies to a polydisperse solution of rodlike micelles and is valid for rods with an axial ratio f (long to short axis) of >3.[1] The viscosity contribution of rods with $f < 3$ is very small. Therefore, it is assumed to be the same as that of spheres.

The viscosity model is applicable if the rods are rigid or only slightly bent and if there is no interaction between the rods (no overlap of rotational volumes). Moreover, the shear applied in the viscometer should be weak enough to prevent shear-induced alignment of the rods. Unless otherwise mentioned, these requirements are met by the experiments that are presented in this paper.

TABLE 2: Values of the Dissociation Constant (K_{diss}) Obtained from Fitting the Rod-Formation Theory to the Viscosity Data for the CpX/KX System

counterion, X	c(X) (mol L^{-1})	K_{diss} (mol L^{-1})
Cl^-	3.5	2.45×10^3
	4.0	2.69×10^3
Br^-	0.4	3.40×10^2
	0.5	4.06×10^2
I^-	0.008	5.0
	0.010	6.1
NO_3^-	0.2	1.83×10^2
	0.4	3.10×10^2

5. Results and Discussion

In Figure 3, theoretical curves and experimental values of the relative viscosity η_{rel} are shown as a function of $\hat{c}_A$ for various systems at different counterion concentrations. Recall that the model has only a single fit parameter, K_{diss}. It should be noted that no agreement between the model and the experimental viscosity data is obtained if the concept of a "dressed micelle" is used[16,39,40]—that is, if direct counterion adsorption is completely excluded. In this case, given by $K_{diss} = \infty$, mainly spherical micelles are obtained, which lead to theoretical curves of viscosity versus surfactant concentration that are much too flat. The theoretical results of Figure 3 are for a system that contains spheres, dumbbells, and rod-shaped micelles of type 1. This system is called model 1. When rod-shaped micelles of type 2 are used, the system is called model 2. As seen from Figure 3, the dependence on $\hat{c}_A$ and the counterion effect are reproduced quite satisfactorily by model 1. In the case of CpI/KI, the viscosity model reaches its limitations, because of rotation overlap of the rods at concentrations beyond the wavy lines. The fitted values of K_{diss} are listed in Table 2. The table shows that counterion adsorption increases (K_{diss} decreases) in the sequence Cl^-, Br^-, NO_3^-, and I^-. This finding is consistent with the Hofmeister series.[41] Table 2 shows that the fitted values of K_{diss} for a given species become greater when the counterion concentration is increased. This is a formal adjustment of the system and should not be considered as a physical feature. The adjustment is necessitated by an extremely high sensitivity of the model to minor changes in molecular energies. To illustrate the sensitivity, let us analyze the system $CpNO_3/KNO_3$ in more detail. For simplicity, very long, rod-shaped micelles with $n_{rod} \gg 10\,000$ are considered. In such long rods, we have $g_c \approx g_c^\infty$; therefore, ΔG_{rod} is virtually identical with the energy required for formation of the endcaps. At $c(NO_3^-) = 0.2$ mol L^{-1}, the fit yields $K_{diss} = 1.83 \times 10^2$ mol L^{-1} and $\Delta G_{rod} = 20.25kT$ (see Figure 3). If this value of K_{diss} is retained and $c(NO_3^-)$ increased to 0.4 mol L^{-1}, a value of $\Delta G_{rod} = 27.48kT$ is obtained after minimization. However, this value leads to η_{rel} values that are far above the experimental value. To re-establish agreement between theory and experiment, at least formally, at $c(NO_3) = 0.4$ mol L^{-1}, K_{diss} must be increased to 3.1×10^2 mol L^{-1} (that is, by a factor of 1.7). This leads to $\Delta G_{rod} = 21.34kT$. Compared with the original value, ΔG_{rod} now is lower by $\sim 6kT$. Considered per surfactant ion in the endcaps, this results in a difference of no more than $0.04kT$, which is approximately the order of magnitude of the error involved in the energy calculations. With this in mind, the agreement between theory and experiment can be considered as reasonably good. Although $0.04kT$ is a small difference, the

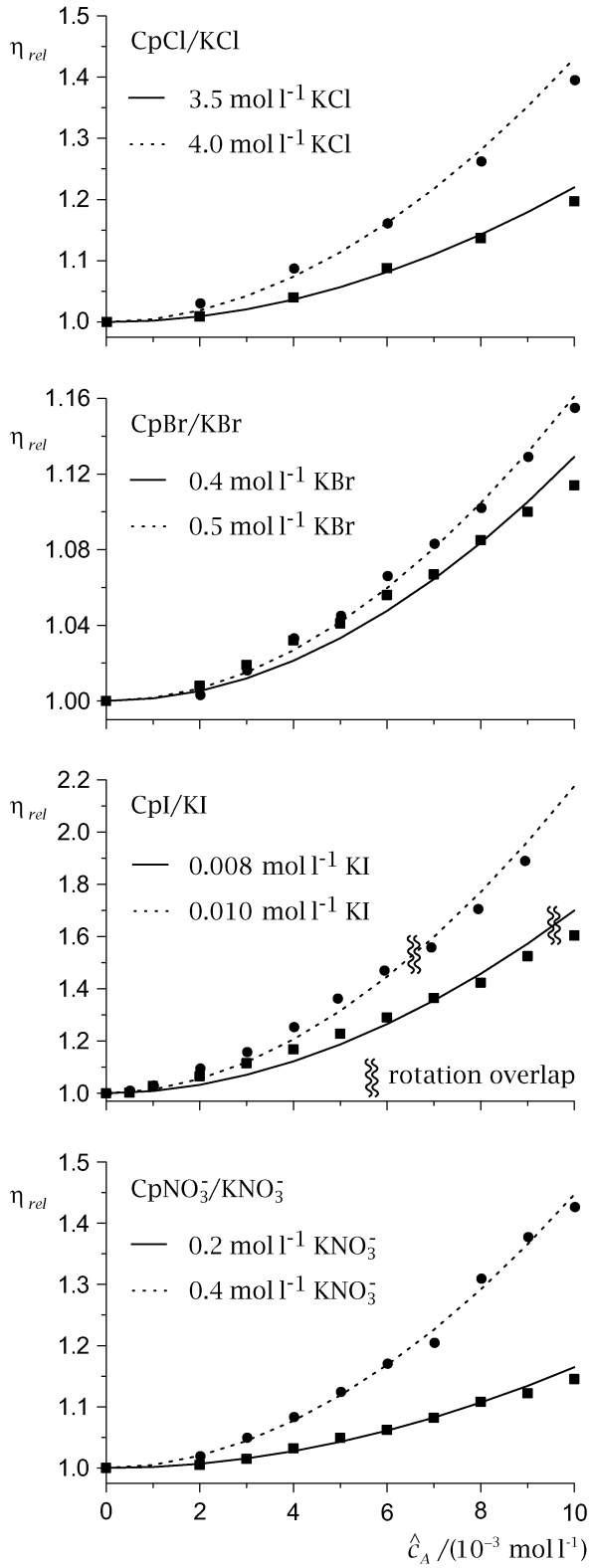

Figure 3. Theoretical curves (lines) and experimental values (symbols) of the relative viscosity (η_{rel}), as a function of $\hat{c}_A$ for different counterions and counterion concentrations. Theoretical curves are calculated from model 1 with the dissociation constant (K_{diss}) values given in Table 2. Rotation overlap can be neglected, except for that in the CpI/KI system, where the beginning of rotation overlap is indicated by the wavy lines.

nature of the energy minimization concept used in the model makes it difficult to reduce it to zero and achieve a reasonable fit of the viscosity curves for both salt concentrations with the same value of K_{diss}. Variations in geometry or parameter values that initially seemed quite promising turned out to be ineffective when the micelle was submitted to the energy minimization procedure. As a result of this procedure, improvements in one degree of freedom were regularly compensated, or even overcompensated, by changes in other degrees of freedom. It seems that further ion-specific effects, such as ionic dispersion forces, must be incorporated into the current model to obtain additional progress.

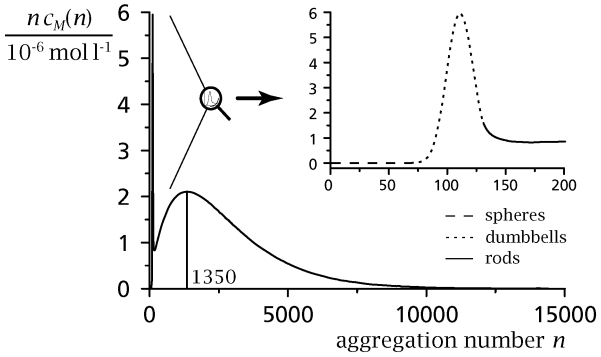

Figure 4. Concentration of surfactant incorporated into micelles of aggregation number n for model 1 and the CpCl/KCl system; $c(Cl^-) = 3.5$ mol L^{-1}, $\hat{c}_A = 8 \times 10^{-3}$ mol L^{-1}, and $K_{diss} = 2.45 \times 10^3$ mol L^{-1}.

TABLE 3: Mean Axial Ratios and Mean Aggregation Numbers for Model 1 and the CpCl/KCl System with $\hat{c}_A = 8 \times 10^{-3}$ mol L^{-1}

$c(Cl^-)$ (mol L^{-1})	3.5	4.0
$\langle f \rangle$	9.9	14.8
$\langle f \rangle_v$	23.1	33.9
$\sigma_v(f)^a$	16.9	24.5
$\langle n \rangle$	1158	1743
$\langle n \rangle_v$	2680	3958
$\sigma_v(n)^a$	1955	2848

[a] $\sigma_v(x)$ is the mean variation of the volume average of x.

In Figure 4, the distribution of the surfactant over spheres, dumbbells, and rods is shown as a function of the aggregation number. Model 1 is used for the CpCl/KCl system with $c(Cl^-) = 3.5$ mol L^{-1} and $\hat{c}_A = 8 \times 10^{-3}$ mol L^{-1}. The concentration of surfactant incorporated into dumbbells is 0.16×10^{-3} mol L^{-1}, and that which is incorporated into rods is 7.84×10^{-3} mol L^{-1}. The amount incorporated into the spheres is negligibly small. The maximum concentration of rods is observed at $n_{rod} = 1350$. Mean aggregation numbers and mean axial ratios for this system, as well as for a system with $c(Cl^-) = 4.0$ mol L^{-1} (K_{diss} from Table 2), are listed in Table 3. An increase of counterion concentration is observed to lead to greater mean aggregation numbers and axial ratios, in addition to a broader distribution of micelles.

Note that the characteristics of the system are strongly influenced by the model geometry used for the rod. In Figure 5, the distribution of micelles is shown for model 2 (with rod-shaped micelles of type 2), with the same concentrations as those used in Figure 4. Curve fitting here leads to $K_{diss} = 1.53 \times 10^3$ mol L^{-1}. The fact that counterion adsorption is stronger than that in model 1 favors the cylindrical geometry, in comparison to spherical geometry. Therefore, dumbbells have almost disappeared and the characteristics of the system at low aggregation numbers have become quite different, compared to those of model 1. Moreover, a higher mean aggregation number and a broader distribution of micelles is obtained.

As a further possible geometrical structure, we have considered a rod-shaped micelle that contains catenoidal parts, as

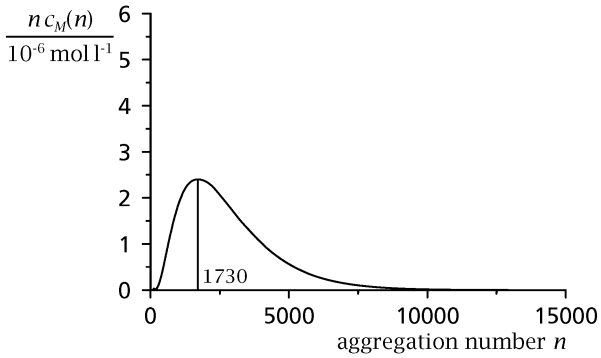

Figure 5. Concentration of surfactant incorporated into micelles of aggregation number n for model 2 and the CpCl/KCl system; $c(Cl^-) = 3.5$ mol L^{-1}, $\hat{c}_A = 8 \times 10^{-3}$ mol L^{-1}, and $K_{diss} = 1.53 \times 10^3$ mol L^{-1}.

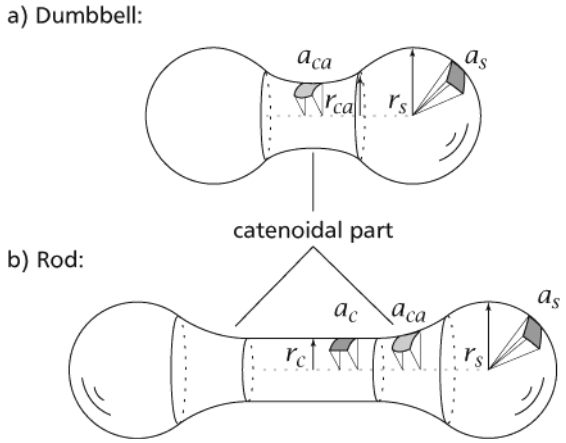

Figure 6. Micellar geometries with a connecting catenoidal component.

proposed in ref 30 (see Figure 6). For this type of micelle, a smooth transition between the cylindrical portion of a rod and the adjacent endcap is created. For the dumbbell, the catenoidal part is intercalated between the endcaps. With respect to conformational energy, the catenoidal portion is modeled as a cylinder of the same volume and length, with respect to electrostatic energy as a plane (because the mean curvature of a catenoid is zero). However, because of the high electrostatic contribution of the "plane" surface elements in the catenoidal portion, curve fitting fails throughout, irrespective of the counterion concentration. Despite this finding, we believe that the counterion concentration problem can be solved by improving the modeling of both chain conformations and electrostatics at the junction between the cylindrical and spherical portions of a rod. Perhaps the minimization procedure for the micelle endcaps that was recently proposed by May and Ben-Shaul[42] might lead to improvements.

Micellar parameters for the CpCl/KCl system for $c(Cl^-) = 3.5$ mol L^{-1} and $c(Cl^-) = 4.0$ mol L^{-1} are listed in Table 4 for a rod of aggregation number $n = 1350$ and a dumbbell of aggregation number $n = 111$. The length of the rod is 74 nm. The geometry scarcely changes when the counterion concentration is increased. The degrees of counterion adsorption increase by ~1%, and the surface potentials decrease by 1−2 mV. For the dumbbell, r_c is similar to r_s, which means that it is only slightly constricted. The parameter a_{dum} is the same as a_{cap} for the rod. Again, the counterion concentration has little influence on the geometry and the degree of adsorption.

TABLE 4: Micellar Parameters for Model 1 and the CpCl/KCl System[a]

	rod		dumbbell	
$c(Cl^-)$ (mol L^{-1})	3.5	4.0	3.5	4.0
K_{diss} (10^3 mol L^{-1})	2.450	2.690	2.450	2.690
r_c (nm)	1.621	1.626	1.912	1.918
a_c (nm^2)	0.575	0.574		
r_s (nm)	2.003	2.006	2.028	2.031
$a_{cap,dum}$ (nm^2)	0.623	0.622	0.621	0.621
n_{cap}	128.5	129.0		
θ_c	0.340	0.348		
$\theta_{cap,dum}$	0.276	0.285	0.280	0.288
$\varphi_{\Phi,c}$ (mV)	188.6	187.8		
$\varphi_{\Phi,cap,dum}$ (mV)	187.7	186.8	188.1	187.0

[a] The rod and the dumbbell have aggregation numbers of 1350 and 111.

6. Conclusions

In summary, we have eliminated five parameters from the previous theory of micelle formation by introducing a physically based model for the conformational energy of the surfactant chain and an improved model for the electrostatic energy of the charged interface. In the new micelle formation model, the counterion dissociation constant is the only free parameter for curve fitting. The model successfully describes the dependence of the micellar size distribution on surfactant concentration and counterion species. It overestimates the effect of changes of the counterion concentration. By formally admitting a dependence of the dissociation constant (K_{diss}) on counterion concentration, our model provides an empirical description of the effect of counterion concentration on micelle formation. Of course, the model also can be applied to other systems where rod formation is dependent on the counterion identity (for instance, the alkali-metal ion/alkyl sulfate system[24]).

In the future, the sensitivity of the model toward a change in counterion concentration must be reduced. For that purpose, the modeling of conformational and electrostatic energy in the transition region between the cylindrical portion and endcaps of the rod must be improved. Moreover, further ion-specific effects should be taken into consideration. For instance, the inclusion of Debye−Hueckel interionic effects might lead to improvements.[43] However, we expect that ionic dispersion forces are more important. As shown recently, ionic dispersion forces have a strong influence on the counterion condensation on spherical micelles[44] and cylindrical polyelectrolytes.[45] In our current work, we have tried to incorporate these forces into an extended version of the present model. With the extended model, the importance of the various counterion specific effects can be easily assessed, simply by switching them on and off.

Acknowledgment. We thank the Deutsche Forschungsgemeinschaft (DFG) for providing financial support.

Appendix: Refined Chain Model and Micellar Geometry

For a given micellar radius R, the micellar core is divided up into L layers concentric to the micelle's surface:

$$L = \frac{R}{d} - 1 \tag{41}$$

where d is the layer width, which was set to 0.154 nm. The layers are numbered, starting with $i = 1$ for the surface layer to

$i = \mathrm{L}$ for the innermost layer. The radius of the outer edge of layer i (r_i) is given by

$$r_i = R - (i-1)d \tag{42}$$

The volume of layer i per surfactant chain (m_i) is given by

$$m_i = \frac{r_i^2 - r_{i+1}^2}{R^2} v_{\mathrm{chain}} \qquad \text{(cylinder)} \tag{43a}$$

$$m_i = \frac{r_i^3 - r_{i+1}^3}{R^3} v_{\mathrm{chain}} \qquad \text{(sphere)} \tag{43b}$$

where v_{chain} is the chain volume.

The surfactant molecule is an *n*-alkane with the structural formula $\mathbf{H}C_nH_{2n+1}$, where **H** is the hydrophilic headgroup. The headgroup does not affect the model, because it is attached outside the micellar core and, therefore, is neglected. The amphiphilic chain, C_nH_{2n+1}, is modeled as a set of C−C bond vectors. The C−C bond length is 0.154 nm, and the C−C−C bond angle 110°. The chain segments are modeled as spheres and placed on the tips of the bond vectors. The diameter of the spheres is taken slightly smaller than the C−C bond length. For the methylene group, two bond vectors are used, with the second always placed in trans conformation.

The chain volume (v_{chain}) is given by

$$v_{\mathrm{chain}} = v_{\mathrm{CH_3}} + (n-1)v_{\mathrm{CH_2}} \tag{44}$$

For a temperature of $T = 323.15$ K, the volumes of the methyl group ($v_{\mathrm{CH_3}}$) and of the methylene group ($v_{\mathrm{CH_2}}$) are taken as 57.7 and 27.3 Å^3, respectively.[25] The volume of the methylene group is assigned to one sphere, and the volume of a methyl group is assigned to two spheres. From geometrical considerations, the maximum length of the surfactant chain (l_{max}) is obtained as

$$l_{\mathrm{max}}(\mathrm{nm}) = (1+n)\,0.154\,\sin(55°) + 0.077$$
$$= 0.126n + 0.203 \tag{45}$$

For a C_{16} chain, $l_{\mathrm{max}} = 2.22$ nm.

A conformation α is characterized by the bond vector $\vec{b}$ leading from the headgroup to the first methylene segment, a bond sequence γ, and a position where the chain is attached to the micelle. The variable $\vec{b}$ is specified by three Euler angles (see Figure 7) and represents the overall orientation of the chain, with respect to the micelle surface. Eighty four different first-bond vectors were used for our calculation. A large number of first-bond vectors improves the smoothness of the curves, but it also increases the computational expense. The bond sequence γ defines the relative positions of the following bond vectors, with respect to $\vec{b}$, and is specified by $(n-1)$ rotational isomeric states. With the rotational isomeric state (ris) approximation, all possible conformations of three consecutive C−C bonds are reduced to three states: trans, gauche$^+$, and gauche$^-$ conformations. Ben-Shaul et al.[35] allowed the chain to be placed within a certain interval around the micelle surface at different positions. Assuming the micelle surface to be flat, we prefer to attach the chain exactly at the micelle surface.

Conformations that have one or more segments with a center of mass outside the micellar core are discarded. For all other conformations, the volume of the surfactant chain is assigned to the different layers of the micelle. A chain-segment sphere is dissected if it lies in different layers. The volumes of the pieces are assigned to the corresponding layers, as shown in Figure 7.

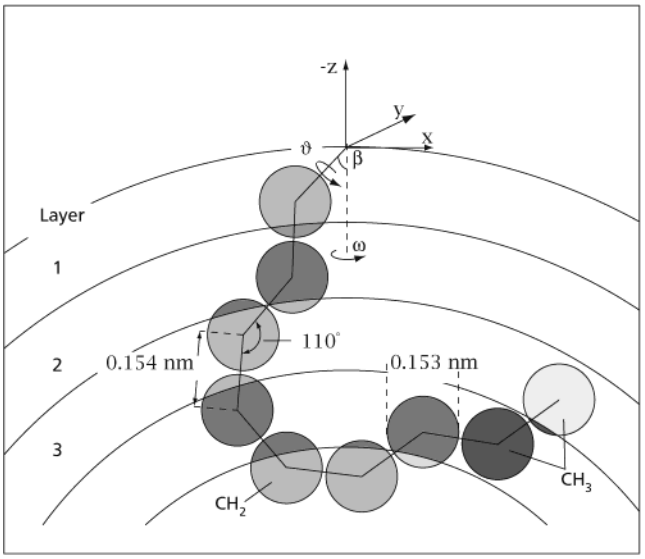

Figure 7. Chain model.

The internal energy of a conformation α is taken as

$$\epsilon(\alpha) = (2094\ \mathrm{J\ mol^{-1}})n_{\mathrm{g}} \tag{46}$$

where n_{g} is the number of gauche conformations of a conformation $\alpha = \{\vec{b},\gamma\}$.

To obtain a more-realistic chain model, conformations with consecutive gauche$^+$/gauche$^+$ or gauche$^-$/gauche$^-$ internal bond sequences are excluded. Thus, the self-overlap of chain segments within the same chain is, for the most part, prevented.

References and Notes

(1) . Kohler, H.-H.; Strnad, J. *J. Phys. Chem.* **1990**, *94*, 7628.
(2) Ekwall, P.; Mandell, L.; Solyom, P. *J. Colloid Interface Sci.* **1971**, *35*, 519.
(3) Porte, G.; Poggi, Y.; Appell, J.; Maret, G. *J. Phys. Chem.* **1984**, *88*, 5713.
(4) Gamboa, C.; Sepúlveda, L. *J. Colloid Interface Sci.* **1986**, *113*, 566.
(5) Gamboa, C.; Ríos, H.; Sepúlveda, L. *J. Phys. Chem.* **1989**, *93*, 5540.
(6) Zoeller, N.; Blankschtein, D. *Langmuir* **1998**, *14*, 7155.
(7) Evans, D. F.; Allen, M.; Ninham, B. W.; Fouda, A. *J. Solution Chem.* **1984**, *13*, 87−101.
(8) Brady, J. E.; Evans, D. F.; Warr, G. G.; Grieser, F.; Ninham, B. W. *J. Phys. Chem.* **1986**, *90*, 1853−1859.
(9) Anacker, E. W.; Ghose, H. M. *J. Am. Chem. Soc.* **1968**, *90*, 3161.
(10) Bayer, O.; Hoffmann, H.; Ulbricht W.; Thurn, H. *Adv. Colloid Interface Sci.* **1986**, *26*, 177.
(11) Mazer, N. A. In *Dynamic Light Scattering*; Pecora, R., Ed.; Plenum Press: New York, 1983; Chapter 8.
(12) Gomati, R.; Appell, J.; Bassereau, P.; Marignan, J.; Porte, G. *J. Phys. Chem.* **1987**, *91*, 6203.
(13) Dörfler, H.-D.; Görgens, C. *Tenside, Surfactants, Deterg.* **2000**, *37*, 96.
(14) Appell, J.; Marignan, J. *J. Phys. II* **1991**, *1*, 1447.
(15) Kalus, J.; Hoffmann, H.; Reizlein, K.; Ulbricht, W.; Ibel, K. *Ber. Bunsen−Ges. Phys. Chem.* **1982**, *86*, 37.
(16) Hayter, J. B. *Langmuir* **1992**, *8*, 2873−2876.
(17) Magid, L. J.; Gee, J. C.; Talmon, Y. *Langmuir* **1990**, *6*, 1609.
(18) Swanson-Vethamuthu, M.; Almgren, M.; Karlsson, G. *Langmuir* **1996**, *12*, 2173.
(19) Wang, K.; Karlsson, G.; Almgren, M. *J. Phys. Chem. B* **1999**, *103*, 9237.
(20) Israelachvili, J. N.; Mitchell, D. J.; Ninham, B. W. *J. Chem. Soc., Faraday Trans. 2* **1976**, *72*, 1525.
(21) Mitchell, D. J.; Ninham, B. W. *J. Chem. Soc., Faraday Trans. 2* **1981**, *77*, 601.
(22) Eriksson, J. C.; Ljunggren, S. *J. Chem. Soc., Faraday Trans. 2* **1985**, *81*, 1209.

(23) Eriksson, J. C.; Ljunggren, S. *Langmuir* **1990**, *6*, 895.
(24) Missel, P. J.; Mazer, N. A.; Carey, M. C.; Benedek, G. B. *J. Phys. Chem.* **1989**, *93*, 8354.
(25) Nagarajan, R.; Ruckenstein, E. *Langmuir* **1991**, *7*, 2934.
(26) Puvvada, S.; Blankschtein, D. *J. Chem. Phys.* **1990**, *92*, 3710.
(27) Thomas, H. G.; Lomakin, A.; Blankschtein, D.; Benedek, G. B. *Langmuir* **1997**, *13*, 209.
(28) Schiloach, A.; Blankschtein, D. *Langmuir* **1998**, *14*, 7166.
(29) Reif, I.; Mulqueen, M.; Blankschtein, D. *Langmuir* **2001**, *17*, 5801.
(30) Heindl, A.; Kohler, H.-H. *Langmuir* **1996**, *12*, 2464.
(31) Evans, F. D.; Ninham, B. W. *J. Phys. Chem.* **1983**, *87*, 5025.
(32) Ninham, B. W.; Yaminski, V. *Langmuir* **1997**, *13*, 2097−2108.
(33) Woelki, S.; Kohler, H.-H. *Chem. Phys.* **2000**, *261*, 411−419.
(34) Woelki, S.; Kohler, H.-H. *Chem. Phys.* **2000**, *261*, 421−438.
(35) Ben-Shaul, A.; Gelbart, W. M. In *Micelles, Membranes, Microemulsions and Monolayers*; Gelbart, W. M., Ben-Shaul, A., Roux, D., Eds.; Springer−Verlag: New York, 1994; Chapter 1.
(36) Volmer, M. *Z. Phys. Chem.* **1925**, *115*, 253.
(37) Marcus, Y. *Ion Solvatation*; Wiley and Sons: New York, 1985; p 100.
(38) Bell, G. M.; Levine, S. In *Chemical Physics of Ionic Solutions*; Conway, B. E., Barradas, R. G., Eds.; Wiley and Sons: New York, 1966; p 409.
(39) Evans, D. F.; Mitchell, D. J.; Ninham, B. W. *J. Phys. Chem.* **1984**, *88*, 6344−6348.
(40) Mohanty, U.; Ninham, B. W.; Oppenheim, I. *Proc. Natl. Acad. Sci. U.S.A.* **1996**, *93*, 4342−4344.
(41) Wennerström, H. *The Colloidal Domain: Where Physics, Chemistry, Biology, and Technology Meet*; VCH: New York, 1994; p 127.
(42) May, S.; Ben-Shaul, A. *J. Phys. Chem. B* **1990**, *105*, 630−640.
(43) Spitzer, J. J. *Colloid Polym. Sci.* **2003**, *281*, 589−592.
(44) Boström, M.; Williams, D. R. M.; Ninham, B. W. *Langmuir* **2002**, *18*, 6010−6014.
(45) Boström, M.; Williams, D. R. M.; Ninham, B. W. *J. Phys. Chem. B* **2002**, *106*, 7908−7912.